COMPARATIVE STUDY OF DIRECT TORQUE CONTROL AND FIELD-ORIENTED CONTROL FOR SIX-PHASE PERMANENT MAGNET SYNCHRONOUS MOTOR

Thi-Anh-Em Bui[1]*, Trong Hai Nguyen[1], Hoang Than[2], Dai-Qui Vo[3], Quoc Thien Pham[1]

[1]Institute of Engineering, HUTECH University, Ho Chi Minh City, Vietnam
[2]Hue Industrial College, Hue City, Vietnam
[3]The University of Danang - University of Science and Technology, Da Nang City, Vietnam

*Corresponding author: bta.em@hutech.edu.vn

(Received: September 09, 2025; Revised: December 05, 2025; Accepted: December 12, 2025)

DOI: 10.31130/ud-jst.2025.23(12).461E

Abstract - This study presents a MATLAB-based comparative simulation of a six-phase Permanent Magnet Synchronous Motor (PMSM) under field-oriented control (FOC) and direct torque control (DTC). The results show that FOC maintains a more stable speed response than DTC, exhibiting smaller errors and reduced ripple, particularly during rapid acceleration steps. Mean torque and RMS fluctuation analyses indicate that FOC delivers smoother torque with significantly lower short-term oscillations, whereas DTC provides a faster torque transient at the expense of larger torque fluctuations, especially at low and medium speeds. Phase-current evaluation further confirms improved current regulation with FOC, with RMS and peak-to-peak values lower or comparable to those of DTC at high speed, reflecting reduced oscillatory behavior. These trends remain consistent across 0–3000 rpm, highlighting the trade-off between the faster torque response of DTC and the smoother torque and current performance of FOC in multiphase PMSM drives.

Key words - Direct Torque Control (DTC); Electric drive systems; Field-Oriented Control (FOC); Permanent Magnet Synchronous Motor (PMSM)

1. Introduction

Permanent magnet synchronous motor (PMSM) has become a central choice in modern high-performance electric drive systems due to their high power density, efficiency, and controllability. In particular, PMSM are widely employed in large-scale electric propulsion systems such as electric vehicles (EVs), aircraft actuators, wind energy conversion systems, and industrial automation, with stringent requirements on reliability and energy efficiency [1, 2]. With the increasing demand for high-power and safety-critical applications, multiphase configurations, especially six-phase PMSM, have been attracting significant research interest. Compared with conventional three-phase machines, six-phase PMSM offer several advantages, including reduced current per phase for the same output power, lower torque ripple, improved fault tolerance under open-phase or short-circuit faults, and enhanced thermal performance [3, 4]. Owing to these advantages, six-phase PMSM are regarded as particularly suitable for mission-critical and heavy-duty applications demanding uninterrupted operation and high reliability.

Controlling a six-phase PMSM is more complex compared with a three-phase machine. In addition to the conventional d–q axis decomposition, the six-phase configuration introduces extra subspaces, including the zero-sequence (z) component and secondary orthogonal components, which must be properly managed to guarantee stable and efficient operation [5]. The complexity demands advanced control algorithms capable of delivering fast dynamic response, accurate torque regulation, and smooth current waveforms simultaneously. Among the control approaches proposed for PMSM, two strategies are widely recognized as state-of-the-art in high-performance drives, namely Direct Torque Control (DTC) and Field-Oriented Control (FOC).

DTC is well recognized for delivering extremely fast torque response with a simple control structure, achieved through direct manipulation of stator flux and torque without current controllers or coordinate transformations [6]. The main advantages include robustness, straightforward implementation, and suitability for real-time applications requiring rapid torque variation. However, DTC also presents drawbacks, including variable switching frequency, elevated torque and flux ripples, and difficulties in preserving the harmonic quality of phase currents. The limitations become particularly critical in high-power six-phase systems, since current quality directly influences electromagnetic compatibility and machine durability. In contrast, FOC has become the benchmark vector control strategy for PMSM, offering smooth current waveforms, decoupled control of flux and torque, and high steady-state performance [7]. By transforming the stator currents into a rotating d–q reference frame aligned with the rotor flux, FOC allows independent regulation of torque-producing and flux-producing components. This leads to excellent dynamic tracking and minimal torque ripple. However, FOC is computationally more demanding, relies on accurate machine parameters, and exhibits slower transient torque response compared to DTC [8]. Thus, a clear trade-off occurs between fast dynamics of DTC and superior current quality of FOC, becoming more pronounced in six-phase systems due to the presence of additional current subspaces.

Recent research on six-phase PMSM has explored various control strategies, with particular attention to dynamic performance, torque ripple minimization, and current quality. Several studies have implemented FOC to achieve smooth phase currents and stable flux control, demonstrating effective torque ripple minimization during steady-state operation [9, 10]. Several studies on DTC

emphasize rapid torque response and robustness against parameter variations, especially under transient conditions [11, 12]. Although prior research provides valuable insights into individual strengths and limitations of DTC and FOC, most investigations evaluate each control method independently and consider a limited range of performance metrics. Several studies primarily assess torque dynamics, whereas others examine current waveform quality or flux stability [13-15]. A systematic investigation is required to compare multiple critical performance metrics, including simultaneous evaluation of rotor speed response, torque ripple, stator flux behavior, and phase current quality, in order to quantify the trade-off between fast torque response and current smoothness in six-phase PMSMs, particularly under identical operating conditions. In addition, six-phase configurations provide extra degrees of freedom for control, yet a comprehensive, side-by-side analysis of DTC and FOC encompassing all relevant performance metrics remains unavailable, serving as the motivation for the present study. In this work, the comparison is deliberately restricted to the conventional implementations of DTC and FOC, which remain the most widely deployed control strategies in industrial PMSM drive systems. Advanced control schemes such as model-predictive DTC, virtual or extended voltage-vector modulation, and parameter-adaptive FOC have recently been proposed for multi-phase traction drives and dual three-phase PMSMs [11-15]. These controllers typically build upon classical DTC/FOC structures and introduce additional prediction horizons, cost functions, or modulation layers, which require a dedicated analysis and careful tuning to ensure a fair comparison. Establishing a clear and quantitative baseline for conventional DTC and FOC under identical six-phase traction-like operating conditions is therefore considered a necessary first step before extending the benchmark to include such advanced strategies.

Several very recent studies have proposed advanced control strategies for six-phase PMSM drives and dual three phase PMSM drives in order to improve torque quality, current quality, and fault tolerance. In [16], finite control set model predictive current control FCS MPCC scheme for six phase PMSM drives is introduced. The control strategy synthesizes virtual voltage vectors and provides simultaneous reduction of current distortion and enhancement of voltage vector selection in the dq and xy subspaces. The reported results indicate significant attenuation of current harmonics together with increased computational cost due to an enlarged vector space and a more complex optimization algorithm. A further line of research, presented in [17], considers a model free predictive flux vector control scheme for N-by-3 phase PMSM systems. The approach combines predictive torque control with a model free design technique and yields fast dynamic response without any requirement for highly accurate machine parameters. The study does not include a direct comparison with conventional field-oriented control in a six-phase configuration.

For dual three-phase PMSM drives, Sun et al., [18] proposes a new MPCC strategy with explicit consideration of common mode voltage CMV and current harmonics. The control scheme employs dedicated virtual voltage vectors and provides CMV reduction together with simplification of the cost function. The proposed formulation highlights advantages of predictive control in multiphase systems, while the main focus remains CMV suppression rather than a comprehensive evaluation of torque and current performance indices in traction operation. In addition, Yao et al., [19] develops a fault tolerant MPCC method for six-phase PMSM drives. The method uses twenty four virtual voltage vectors for voltage vector compensation under single phase open circuit faults and preserves decoupling between subspaces together with balanced currents in the remaining windings. The reported findings demonstrate strong potential of predictive control for six-phase traction drive applications, particularly under faulty conditions, while most studies emphasize fault tolerant scenarios rather than comparisons with conventional DTC and FOC structures in healthy operation.

For high power traction applications, Kuang et al., [20] analyzes drive control technology for dual three-phase PMSM in an electric propulsion system for aircraft. The study compares two vector control schemes based on space vector modulation and evaluates their impact on harmonic components and torque quality. The investigation reinforces the role of multiphase drives in safety critical systems but considers only one class of advanced vector control schemes and does not include any direct comparison with DTC. Overall, the available studies concentrate on advanced control structures such as MPCC, model free predictive control, and optimized SVM for six-phase or dual three-phase PMSM, usually under specific scenarios such as CMV reduction, fault tolerant operation, or current harmonic optimization. The literature does not provide a quantitative benchmark with parallel evaluation of conventional DTC and FOC for the same six-phase machine and identical traction load conditions.

In comparison with recent studies, the present paper concentrates on construction of a clear quantitative baseline for two classical control structures DTC and FOC applied to the same six phase PMSM drive configuration with an identical speed profile oriented toward traction applications. A joint analysis of speed response indices, torque ripple, and phase current quality under identical operating conditions enables clarification of the trade off between fast torque response associated with DTC and high current smoothness associated with FOC. Advanced control strategies such as MPCC, model free predictive control, and optimal modulation do not form part of the comparison in the present study and the evaluation remains limited to simulation results, representing methodological limitations of the work. By providing a clear DTC and FOC benchmark for a six phase PMSM drive, the obtained results supply a necessary reference point for future studies with extensions of the baseline toward predictive control, fault tolerant operation, or optimization oriented design for multiphase traction drives.

The objective of this study is to conduct a comparative analysis of DTC and FOC control strategies applied to a six-phase PMSM. The evaluation focuses on three key performance indicators: speed tracking accuracy, torque response and ripple, and phase current quality. A

MATLAB-based simulation framework with realistic motor parameters is used to systematically compare performance and investigate the trade-offs between rapid torque response and smooth current waveforms. The study provides insights for selecting appropriate control strategies in multi-phase PMSM drive applications.

2. System description

2.1. Machine and System Parameters

A six-phase PMSM with a dual three-phase winding configuration is the focus of this study. Two three-phase stator windings are spatially displaced by 30 electrical degrees, enhancing fault tolerance, the lowering phase current per winding, and improving torque capability. Compared with conventional three-phase machines, the motor provides better reliability and performance. Table 1 shows key electrical and mechanical parameters, including DC-link voltage, rotor inertia, number of pole pairs, stator resistances, and inductances. The listed parameters define the fundamental characteristics of the motor. The set of parameters provides a reference for constructing the mathematical model and implementing the control strategy. Accurate specification ensures that simulation results reflect the dynamic behavior of the six-phase PMSM system.

Table 1. *PMSM and control parameters used in the simulations*

Parameter	Symbol	Value	Unit
d-axis inductance	L_d	0.00024368	H
q-axis inductance	L_q	0.00029758	H
Zero-sequence inductance	L_0	0.00012184	H
Resistance	R_s	0.010087	Ω
Permanent magnet flux	ψ_m	0.04366	Wb
Pole pairs	p	8	-
Rotor inertia	J_m	0.1234	kg·m²
DC link voltage	V_{dc}	600	V
Sampling time	T_s	5e-6	s
Speed controller gains	K_p/K_i	4.5/300	-

2.2. Mathematical Model of Six-Phase PMSM

The dynamic behavior of the six-phase PMSM can be described by electrical and mechanical equations [5]. The model is usually formulated in the natural *abcdef* frame and then transformed into two sets of orthogonal *dq* frames through the Park transformation. The transformation enables the decoupling into two equivalent three-phase subsystems, thereby simplifying the control design.

2.2.1. Voltage equations in the natural frame

$$\begin{bmatrix} v_a \\ v_b \\ v_c \\ v_d \\ v_e \\ v_f \end{bmatrix} = R_s \begin{bmatrix} i_a \\ i_b \\ i_c \\ i_d \\ i_e \\ i_f \end{bmatrix} + \frac{d}{dt} \begin{bmatrix} \psi_a \\ \psi_b \\ \psi_c \\ \psi_d \\ \psi_e \\ \psi_f \end{bmatrix} \quad (1)$$

where v_x, i_x, ψ_x ($x = a \ldots f$) are the stator phase voltages, currents, and flux linkages, respectively, and R_s is the stator resistance.

2.2.2. Voltage equations in the dq synchronous frame

$$\begin{cases} v_d = R_s i_d + \dfrac{d\psi_d}{dt} - \omega_e \psi_q \\ v_q = R_s i_q + \dfrac{d\psi_q}{dt} - \omega_e \psi_d \end{cases} \quad (2)$$

where v_d, v_q are the dq-axis voltages; i_d, i_q are the currents; ψ_d, ψ_q are the *flux* linkages and ω_e is the electrical angular speed.

2.2.3. Flux linkage relations

$$\begin{cases} \psi_d = L_d i_d + \psi_f \\ \psi_q = L_q i_q \end{cases} \quad (3)$$

where L_d and L_q are the *d-axis* and *q-axis* inductances, and ψ_f is the flux linkage generated by the permanent magnets.

2.2.4. Mechanical dynamics

$$J\frac{d\omega_m}{dt} = T_e - T_L - B\omega_m \quad (4)$$

where J is the rotor inertia, ω_m is the mechanical angular speed, T_L is the load torque, and B is the viscous friction coefficient. The electromagnetic torque is expressed as:

$$T_e = \frac{3p}{2}\left(\psi_d i_d + \left(\psi_q - L_q i_q\right) i_q\right) \quad (5)$$

where p is the number of pole pairs. In the case of a six-phase PMSM, the total electromagnetic torque is obtained by summing the contributions of the two decoupled *dq* subsystems.

2.3. Power Converter and Load

The six-phase PMSM under study is supplied by a dual three-phase voltage source inverter (VSI). The inverter comprises two conventional three-phase bridges connected in parallel, and each bridge feeds one three-phase winding set of the machine with a spatial phase displacement of 30°. The arrangement generates two balanced three-phase systems, and the systems can be modulated independently or controlled jointly depending on the employed strategy [21-23].

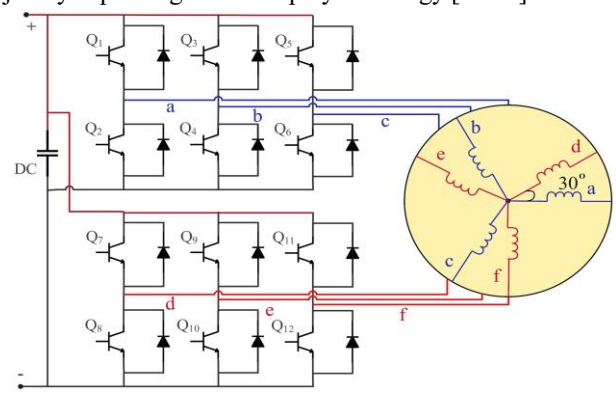

Figure 1. *Schematic diagram of the six-phase PMSM and the dual three-phase inverter*

For dynamic evaluation of the proposed drive system, a step speed reference profile is employed. The reference speed is increased in steps (for example, from 500 rpm to 2000 rpm and 3000 rpm) under both no-load and load torque conditions, enabling an assessment of the transient and steady-state performance of the controller. The

external load torque is applied either as a constant disturbance or as a step change to examine the robustness of the control scheme under varying operating conditions. A schematic diagram of the dual three-phase inverter supplying the six-phase PMSM is presented in Figure 1.

3. Control strategies

Figure 2 illustrates block diagrams of DTC and FOC strategies for a six-phase PMSM with a dual three-phase inverter. DTC and FOC represent two widely applied control methods in multiphase PMSM drives. The following subsections provide a detailed explanation of each method.

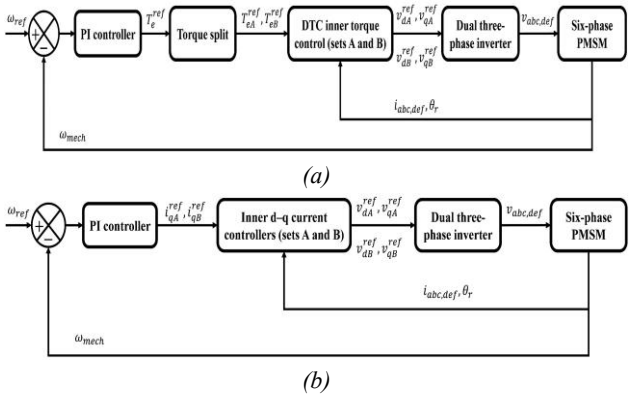

(a)

(b)

Figure 2. *Block diagrams of the DTC (a) and FOC (b) strategies for a six-phase PMSM with a dual three-phase inverter*

3.1. Direct Torque Control

DTC enables fast dynamic response and removes the need for intermediate current loops. The electromagnetic torque T_e and the stator flux magnitude ψ_s are controlled directly through optimal voltage vectors selected from a lookup table. The lookup table maintains variable states within predefined hysteresis bands, minimizing torque and stator current ripple without intermediate current controllers.

In this work, a simplified DTC variant is adopted and adapted to the six-phase PMSM traction drive. The electromagnetic torque is directly controlled by a non-linear torque error law with a deadband threshold, while the stator flux magnitude is adjusted indirectly through a field-weakening law acting on the d-axis current. The inner control structure does not include any intermediate d–q current PI loops.

Let $k \in \{A, B\}$ denote the two stator sets associated with windings *abc, def,* respectively. For each set, the torque error is defined as the difference between the reference and the estimated electromagnetic torque, i.e.

$$\Delta T_{ek} = T_{ek}^{ref} - T_{ek}^{est} \tag{6}$$

The estimated torque T_{ek}^{ref} is obtained from the estimated d–q currents and the motor parameters. The sign and magnitude of ΔT_{ek} are then used to determine the q-axis voltage component of each set. When $|\Delta T_{ek}|$ exceeds a prescribed threshold, the corresponding q-axis voltage command is driven to $\pm V_{limit}$; otherwise, it is set to zero. In this way, the electromagnetic torque of each three-phase winding set is directly regulated without resorting to inner current PI controllers.

In parallel, a simple field-weakening strategy is implemented on the d-axis current. For each set, an electrical angular speed is computed from the mechanical speed and the number of pole pairs. Assuming $i_d = 0$, the q-axis voltage required to produce the desired torque is estimated and compared with the effective voltage limit V_{limit}. If the required q-axis voltage exceeds the limit, a negative d-axis current reference is calculated so that the resulting d–q voltage magnitude does not exceed V_{limit}. The d-axis voltage command is then generated to drive the actual d-axis current towards this theoretical field-weakening reference. As a result, the d–q voltage commands $v_{dA}^{ref}, v_{qA}^{ref}, v_{dB}^{ref}, v_{qB}^{ref}$ are obtained for the two three-phase winding sets and subsequently limited in magnitude before being applied to the inverter.

The outer speed loop provides the total torque reference for the DTC block. A PI speed controller compares the reference mechanical speed ω_{ref} with the measured speed ω_{mech}, and generates the total torque reference T_e^{ref}.

$$T_e^{ref} = K_p\left(\omega_{ref} - \omega_{mech}\right) + K_i\int\left(\omega_{ref} - \omega_{mech}\right)dt \tag{7}$$

The torque-splitting block then distributes this reference evenly between the two three-phase winding sets, yielding $T_{eA}^{ref} = T_{eB}^{ref} = 0.5T_e^{ref}$. The overall DTC structure for the six-phase PMSM is summarized in Figure 2(a). The outer PI speed controller receives $\omega_{ref,}$ ω_{mech}, and outputs the total torque reference T_e^{ref}. The Torque split block generates the per-set torque references T_{eA}^{ref} and T_{eB}^{ref}. The DTC inner torque control (sets A and B) block processes these torque references together with the measured phase currents $i_{abc,def}$, the rotor position θ_r and ω_{mech}. Internally, it performs flux and torque estimation, computes the torque errors ΔT_{eA} and ΔT_{eB}, applies the field-weakening law on the d-axis current, and produces the d–q voltage commands $v_{dA}^{ref}, v_{qA}^{ref}, v_{dB}^{ref}, v_{qB}^{ref}$. The dual three-phase inverter converts these commands into the six stator phase voltages $v_{abc,def}$, which excite the six-phase PMSM. The motor generates $i_{abc,def,}$ and ω_{mech}. The phase currents are fed back to the DTC block for flux and torque estimation, while the mechanical speed is fed back to the PI speed controller, thereby closing both the inner torque loop and the outer speed loop.

3.2. Field-Oriented Control

FOC represents a standard vector control strategy for six-phase PMSM. In rotor-flux–aligned d–q coordinates, the stator current is decomposed into a d-axis component, which primarily affects the flux, and a q-axis component, which produces the electromagnetic torque. FOC typically uses a cascaded structure with an outer speed control loop and inner d–q current control loops.

In the six-phase PMSM traction drive considered in this work, FOC is implemented as a cascaded scheme. The inner layer consists of two independent d–q current control loops, one for each three-phase winding set (A and B). From the measured $i_{abc,\ def}$, θ_r, the d–q currents i_{dA}, i_{qB}, i_{dB}, i_{qA} are obtained and compared with their references. PI regulators with decoupling terms then generate the d–q voltage commands $v_{dA}^{ref}, v_{qA}^{ref}, v_{dB}^{ref}, v_{qB}^{ref}$. Feedforward compensation based on the electrical speed and machine

parameters is used to cancel cross-coupling and back-EMF terms, and the resulting voltage vectors are limited according to the available DC bus voltage.

Above the current loops, an outer speed regulation layer shapes the torque demand. The PI controller operates on the speed tracking error ($\omega_{ref} - \omega_{mech}$) and delivers a total torque reference, which is converted into a total q-axis current reference and then split equally between the two three-phase sets to obtain $i_{qA}^{ref}, i_{qB}^{ref}$. In the operating range studied, the d-axis current references are kept at zero for both sets, i.e. $i_{dA}^{ref}, i_{dB}^{ref}$, so that the machine is driven without explicit flux-weakening in the FOC case.

The resulting closed-loop structure is summarised in Figure 2(b). The PI controller block receives ω_{ref} the feedback speed ω_{mech} and provides the per-set q-axis current references i_{qA}^{ref} and i_{qB}^{ref}. The inner d–q current controllers (sets A and B) block uses these references together with $i_{abc,def}$ and θ_r to compute the voltage commands $v_{dA}^{ref}, v_{qA}^{ref}, v_{dB}^{ref}, v_{qB}^{ref}$, which are applied by the dual three-phase inverter to generate the six stator phase voltages $v_{abc,def,}$ feeding the six-phase PMSM. The motor outputs $i_{abc,def}$ and ω_{mech}. The currents are fed back to the inner current controllers and the speed is fed back to the PI controller, thereby closing the inner current loop and the outer speed loop.

4. Results and discussion

4.1. Simulation Setup

The simulation is carried out to evaluate the dynamic performance under realistic operating conditions. The speed reference profile is defined stepwise from 0 to 500 rpm at 0.2 s, then to 2000 rpm at 0.4 s, and finally to 3000 rpm at 0.7 s. A sinusoidal load torque with 40 Nm amplitude and 0.5 Hz frequency is applied. The torque level representing roughly 20% of the motor rated torque is chosen to emulate dynamic load variations and to test the controllers transient responses.

Initial conditions are set as zero currents for both winding sets, i_{dA} i_{qA} i_{dB} i_{qB} equal to zero, and rotor mechanical speed ω_{mech} equal to zero. The simulation runs for 1s with a sampling time of 5 µs, compatible with high-speed PWM implementation. Logged variables include rotor speed, electromagnetic torque, *d-q axis* currents for both winding sets, and phase currents *abc* of all six-phases. The recorded data allow assessment of speed tracking performance, torque ripple, and current waveforms. Both DTC and FOC simulations share the same motor parameters, initial conditions, speed profile, and load torque profile, ensuring a fair comparison of control performance.

4.2. Performance Analysis of DTC and FOC

The dynamic performance of the six-phase PMSM drive under DTC and FOC is investigated at three reference speeds, namely 500, 2000 and 3000 rpm. For each speed condition, the transient response is characterised by the rise time t_r, settling time t_s, overshoot (OS) and steady-state error e_{ss}. Rise time reflects the capability to respond rapidly when the reference speed changes. Settling time indicates the stability of the system once it reaches the desired value. Overshoot represents the oscillation beyond the target and is related to robustness. Steady state error expresses the long-term accuracy of the control method. In steady state, the quality of the torque production and stator currents is assessed through the RMS torque and current ripple. The numerical values of these performance indices are reported in Table 2.

Table 2. *Performance indices of speed response, RMS torque and RMS phase current for the six-phase PMSM drive under DTC and FOC at different reference speeds*

Speed (rpm)	Controller	Speed response				Ripple indices	
		t_r (s)	t_s (s)	os (%)	e_{ss}	RMS torque (Nm)	RMS current (A)
500	DTC	0.041	0.2	-6.5	-6.96	52.73	56
	FOC	0.037	0.044	0.1	-0.15	49.62	63.63
2000	DTC	0.138	0.149	-1.6	-1.58	62.37	105
	FOC	0.134	0.144	0.03	-0.04	60.79	104.94
3000	DTC	0.07	0.084	-0.5	-0.51	69	84.39
	FOC	0.067	0.081	0.03	-0.01	68	82.57

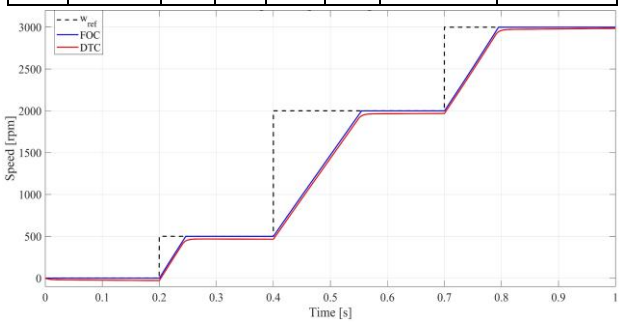

Figure 3. *Speed responses of the six-phase PMSM under DTC and FOC control strategies*

The speed responses indicate that FOC provides faster and more accurate tracking of the reference speed than DTC over the whole investigated range. As summarised in Table 2, the rise time t_r of FOC is slightly shorter than that of DTC at all speed steps. For example, 0.037s versus 0.041s at 500 rpm, while the settling time t_s is significantly reduced at low speed 0.044s versus 0.2s at 500 rpm. In addition, the steady-state error e_{ss} of FOC remains very close to zero, within about ±0.2% for all operating points, whereas DTC exhibits a noticeable negative overshoot and residual speed offset, with e_{ss} around −7 % at 500 rpm and still non-zero at higher speeds. Although the nominal settling times of the two methods become comparable at 2000 and 3000 rpm, the trajectories in Figure 3 show that FOC converges to the reference with smaller deviations and reduced oscillations, resulting in a smoother and more stable speed profile.

The torque characteristics in Figure 4, together with the RMS values in Table 2, highlight the corresponding trade-off in torque ripple. Both strategies are able to track the demanded mean torque over the considered speed range, but FOC generally produces smoother torque. At 500 rpm, the RMS torque ripple under FOC is already slightly lower than under DTC, with values of 49.62 Nm and 52.73 Nm, respectively. The tendency is maintained as the speed increases, and the RMS values decrease from 62.37 Nm (DTC) to 60.79 Nm (FOC) at 2000 rpm and from 69.00 Nm (DTC) to 68.00 Nm (FOC) at 3000 rpm. The

waveforms in Figure 4 confirm that, particularly at medium and high speeds, the electromagnetic torque under FOC exhibits less short-term oscillation, whereas the DTC torque is characterised by sharper pulsations associated with the discrete voltage-vector selection.

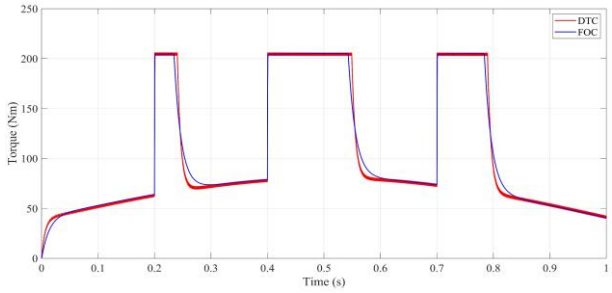

Figure 4. *Electromagnetic torque responses of the six-phase PMSM under DTC and FOC*

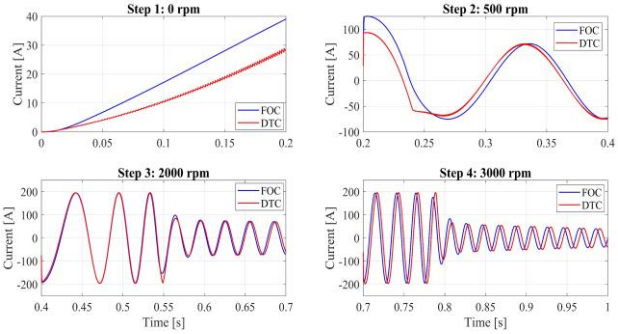

Figure 5. *Representative phase-a current of the six-phase PMSM under DTC and FOC at four speed steps (0, 500, 2000, and 3000 rpm), highlighting the effect of speed on current ripple and mean value*

The phase-current behaviour in Figure 5 follows a similar pattern. At standstill, FOC injects higher mean and RMS phase current due to the action of the outer speed PI controller and the q-axis current loop, which actively maintain the required static torque. The current ripple becomes more favourable under FOC at medium and high speeds. At 500 rpm, the RMS phase current is 63.63 A for FOC and 56.00 A for DTC, whereas from 2000 rpm upwards FOC maintains a slightly lower RMS current than DTC, with values of 104.94 A and 105.00 A at 2000 rpm and 82.57 A and 84.39 A at 3000 rpm for DTC and FOC, respectively, as reported in Table 2. The representative phase currents under FOC therefore exhibit smoother envelopes and reduced short-term oscillations, evidencing improved current regulation and reduced electromagnetic stress on both inverter and PMSM.

For the step load disturbance test, illustrated in Figure 6, the load torque is increased abruptly from 40 Nm to 100 Nm at $t = 0.5$s while the speed reference is kept at 2000 rpm. Both controllers exhibit a pronounced but bounded speed sag after the disturbance. In the interval $t \in [0.5, 0.7]$ second, the maximum speed dip is approximately −1018.6 rpm for FOC and −1044.3 rpm for DTC, corresponding to about −50.9% and −52.2% of the reference speed, respectively. This implies that the rotor speed temporarily decreases to around 981 rpm with FOC and 956 rpm with DTC. Despite these similar peak deviations, the RMS speed error over the same interval is lower for FOC (53.7 rpm) than for DTC (70.8 rpm), which indicates a smoother and better damped recovery. Within the considered time window, neither controller returns to within a ±2% band around 2000 rpm before the next speed step at $t = 0.7$s, since the speed loop operates close to saturation in response to the large increase in load torque. Nevertheless, the FOC strategy consistently yields smaller average speed deviations and less oscillatory behaviour than DTC under the step load disturbance, in agreement with the nominal comparison presented above.

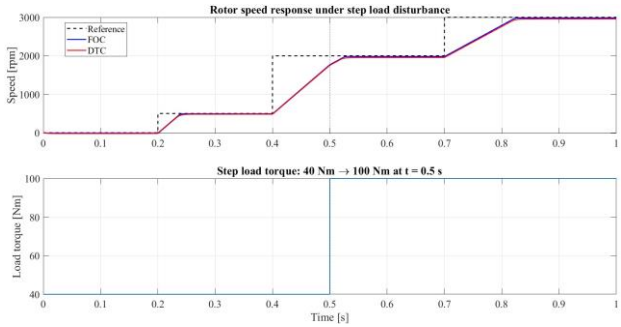

Figure 6. *Speed response of the six-phase PMSM under DTC and FOC and corresponding step load torque profile (40 Nm to 100 Nm at $t = 0.5$ s)*

The behaviours described above can be directly related to the different control structures of DTC and FOC. In FOC, the decoupled d–q current regulators within the cascaded speed–current control loop enforce smooth tracking of the reference currents and flux, which inherently damps torque and current oscillations and minimises the steady-state speed error. In contrast, DTC relies on hysteresis comparators and a switching table to select discrete voltage vectors, leading to abrupt changes in stator voltage and current. This quantised control action provides competitive dynamic response but naturally produces higher torque and current ripple and larger residual speed errors, particularly at low speed where flux estimation and inverter non-idealities have a stronger impact. The additional robustness test with a step increase in load torque from 40 Nm to 100 Nm further confirms these trends, since FOC yields smaller average speed deviations and a better damped recovery than DTC under the same disturbance. It can therefore be concluded that, for the investigated six-phase PMSM drive, FOC achieves a more accurate and stable dynamic response with lower torque and current ripple over the whole operating range, as well as improved robustness to sudden load changes. DTC retains the advantage of a relatively simple structure and good dynamic performance, but this comes at the expense of larger steady-state speed errors and higher torque and current fluctuations, especially in the low- and medium-speed regions and in the presence of abrupt load disturbances.

5. Conclusion

This study compared the dynamic performance of a six-phase PMSM drive under classical DTC and FOC strategies through detailed simulation. The analysis considered multiple speed steps (0, 500, 2000, and 3000 rpm) and evaluated speed tracking, electromagnetic torque ripple, and phase current quality under identical operating

conditions. The results show that FOC consistently provides faster and more accurate speed response, smaller steady-state speed error, and smoother phase currents, while DTC achieves rapid torque response at the cost of increased torque and current ripple. Quantitative comparisons across the investigated speed range confirm that FOC yields lower RMS torque ripple and slightly lower RMS phase currents at medium and high speeds. These findings demonstrate the superior torque stability and current smoothness of FOC, particularly at higher speeds, whereas DTC retains the advantage of a simple structure and competitive dynamic performance but with larger short-term oscillations. An additional robustness test with a step load disturbance, in which the load torque is increased abruptly from 40 Nm to 100 Nm at 2000 rpm, further confirms that FOC produces smaller average speed deviations and a better damped recovery than DTC, in line with the nominal comparison results.

Future research will focus on the experimental validation of the six-phase PMSM control strategies investigated in this study. Implementation of both DTC and FOC on real-time DSP or FPGA platforms will allow the assessment of actual dynamic performance, including speed response, torque tracking, and phase current ripple. The experiments will employ a six-phase PMSM coupled with precise torque and speed sensors, enabling direct comparison with simulation results. Key aspects such as parameter variations, load disturbances, and voltage limitations will be examined to evaluate the robustness and stability of each control strategy. Additionally, iterative tuning of PI gains for FOC and switching parameters for DTC will be performed to optimize torque smoothness and minimise current ripple under real operating conditions. In addition to experimental validation, future work will also extend the present benchmark by incorporating at least one advanced control strategy as an additional reference, for example model-predictive DTC or enhanced FOC schemes with virtual or extended voltage-vector modulation. This will allow a more comprehensive assessment of the performance gap between classical and advanced controllers for six-phase PMSM traction drives. These efforts aim to bridge the gap between simulation and practical performance, providing critical insights for the deployment of six-phase PMSMs in high-precision, high-speed applications.

REFERENCES

[1] D. Mehta, R. Kumar, and P. K. Shah, "Application of Permanent Magnet Synchronous Motors in Electric Drive Systems," in *2024 International Conference on Optimization Computing and Wireless Communication (ICOCWC)*, 2024: IEEE, pp. 1-5.

[2] I. Bolvashenkov *et al.*, "Fault Tolerant Multi-phase Permanent Magnet Synchronous Motor for the More Electric Aircraft," in *Fault-Tolerant Traction Electric Drives: Reliability, Topologies and Components Design*: Springer, 2019, pp. 73-92.

[3] G. Pellegrino, "Six Phase Fractional Slot Surface Permanent Magnet Motor for High Torque Density and High Speed," in *2022 International Conference on Electrical Machines (ICEM)*, 2022: IEEE, pp. 1417-1423.

[4] H. Gao, J. Guo, B. Zhang, and G. Zhang, "Fault-tolerant control technology of symmetrical six-phase permanent magnet synchronous motor," *IET Power Electronics,* vol. 16, no. 1, pp. 37-52, 2023.

[5] J. Y. Su, J. B. Yang, and G. J. Yang, "Mathematical model research of six-phase PMSM," *Advanced Materials Research,* vol. 614, pp. 1266-1271, 2013.

[6] C. Ortega, A. Arias, C. Caruana, J. Balcells, and G. M. Asher, "Improved waveform quality in the direct torque control of matrix-converter-fed PMSM drives," *IEEE Transactions on Industrial Electronics,* vol. 57, no. 6, pp. 2101-2110, 2009.

[7] M. Y. A. Khan, "A Review of Analysis and Existing Simulation Model of Three Phase Permanent Magnet Synchronous Motor Drive (PMSM)," *Control Systems and Optimization Letters,* vol. 2, no. 3, pp. 349-356, 2024.

[8] D. Majchrzak and P. Siwek, "Comparison of FOC and DTC methods for a Matrix Converter-fed permanent magnet synchronous motor," in *2017 22nd International Conference on Methods and Models in Automation and Robotics (MMAR)*, 2017: IEEE, pp. 525-530.

[9] S. Bharti, C. Bhende, and O. Ray, "Control of Six-Phase Permanent Magnet Synchronous Motor for Electric Vehicle Application," in *2022 IEEE 2nd International Conference on Sustainable Energy and Future Electric Transportation (SeFeT)*, 2022: IEEE, pp. 1-6.

[10] P. F. Goncalves, S. M. Cruz, and A. M. Mendes, "Multistage predictive current control based on virtual vectors for the reduction of current harmonics in six-phase PMSMs," *IEEE Transactions on Energy Conversion,* vol. 36, no. 2, pp. 1368-1377, 2021.

[11] X. Ma, Y. Yu, H. Zhang, W. Wang, and L. Liu, "Study on direct torque control of dual Y shift 30 degree six-phase PMSM," in *2015 IEEE 10th conference on industrial electronics and applications (ICIEA)*, 2015: IEEE, pp. 1964-1968.

[12] G. H. B. Foo and X. Zhang, "Constant switching frequency based direct torque control of interior permanent magnet synchronous motors with reduced ripples and fast torque dynamics," *IEEE Transactions on Power Electronics,* vol. 31, no. 9, pp. 6485-6493, 2015.

[13] P. F. Gonçalves, S. M. Cruz, and A. M. Mendes, "Predictive current control of six-phase permanent magnet synchronous machines based on virtual vectors with optimal amplitude and phase," in *2019 International Conference on Smart Energy Systems and Technologies (SEST)*, 2019: IEEE, pp. 1-6.

[14] K. Mohith, S. Patilkulkarni, and N. Kollaparti, "Comparative analysis of different control techniques for six-phase PMSM as an application to HEV," in *Smart Sensors Measurements and Instrumentation: Select Proceedings of CISCON 2020*: Springer, 2021, pp. 93-108.

[15] M. Furmanik, L. Gorel, D. Konvičný, and P. Rafajdus, "Comparative study and overview of field-oriented control techniques for six-phase PMSMs," *Applied Sciences,* vol. 11, no. 17, p. 7841, 2021.

[16] Y. Huang, S. Liu, R. Pang, X. Liu, and X. Rao, "Model Predictive Current Control for Six-Phase PMSM with Steady-State Performance Improvement," *Energies,* vol. 17, no. 21, p. 5273, 2024.

[17] G. Wu, X. Chen, Q. Wu, Z. Long, S. Huang, and C. Zhang, "Model-free predictive flux vector control for N∗ 3-Phase PMSM drives considering parameters mismatch," *International Journal of Electrical Power & Energy Systems,* vol. 160, p. 110079, 2024.

[18] Q. Sun, Z. Zhang, Q. Zhang, and J. Yu, "Model predictive current control for dual three-phase permanent magnet synchronous motor with common-mode voltage suppression," *Journal of Electrical Engineering & Technology,* vol. 19, no. 5, pp. 3203-3216, 2024.

[19] M. Yao, J. Peng, X. Sun, and Y. Sun, "Fault-tolerant model predictive current control of six-phase permanent magnet synchronous motors with pulse width modulation," *Journal of Electrical Engineering & Technology,* vol. 18, no. 3, pp. 1785-1797, 2023..

[20] Z. Zhang, S. Jin, Z. Zhang, F. Zhang, and B. Li, "Novel space vector PWM technology with lower common-mode voltage for dual three-phase PMSM," *IET Power Electronics,* vol. 13, no. 7, pp. 1426-1433, 2020.

[21] L. Xiao, L. Zhang, F. Gao, and J. Qian, "Robust fault-tolerant synergetic control for dual three-phase PMSM drives considering speed sensor fault," *IEEE Access,* vol. 8, pp. 78912-78922, 2020.

[22] L. Li, W. Zhou, X. Bi, X. Sun, and X. Shi, "Second-Order Model-Based Predictive Control of Dual Three-Phase PMSM Based on Current Loop Operation Optimization," in *Actuators*, vol. 11, no. 9: MDPI, p. 251, 2022.